



OPEN ACCESS

EDITED BY

Qinghong Yuan,
East China Normal University, China

REVIEWED BY

Kedhareswara Sairam Pasupuleti,
Chungnam National University, Republic of
Korea
Zheng Guo,
Anhui University, China

*CORRESPONDENCE

Zhigang Zhu,
✉ zhigang_zhu259@163.com

†These authors have contributed equally to
this work

RECEIVED 07 February 2024

ACCEPTED 15 April 2024

PUBLISHED 24 May 2024

CITATION

Han Y, Ding Y, Yao Y, Li Z and Zhu Z (2024),
Heterostructured $Ti_3C_2T_x$ /carbon
nanohorn-based gas sensor for NH_3
detection at room temperature.
Front. Mater. 11:1383538.
doi: 10.3389/fmats.2024.1383538

COPYRIGHT

© 2024 Han, Ding, Yao, Li and Zhu. This is an
open-access article distributed under the
terms of the [Creative Commons Attribution
License \(CC BY\)](#). The use, distribution or
reproduction in other forums is permitted,
provided the original author(s) and the
copyright owner(s) are credited and that the
original publication in this journal is cited, in
accordance with accepted academic practice.
No use, distribution or reproduction is
permitted which does not comply with
these terms.

Heterostructured $Ti_3C_2T_x$ /carbon nanohorn-based gas sensor for NH_3 detection at room temperature

Yutong Han[†], Yuan Ding[†], Yu Yao, Zhanhong Li and
Zhigang Zhu*

School of Health Science and Engineering, University of Shanghai for Science and Technology,
Shanghai, China

In this study, a two-dimensional $Ti_3C_2T_x$ MXene compounded with carbon nanohorn (CNH) by an electrostatic self-assembly method was proposed and then fabricated as room temperature ammonia (NH_3) gas sensors. The successful preparation of the $Ti_3C_2T_x$ /CNH nanocomposite has been characterized in detail. The NH_3 sensing performance based on $Ti_3C_2T_x$ /CNH also has been tested at room temperature. The optimal $Ti_3C_2T_x$ /CNH sensor has a response value of 21.6% to 100 ppm NH_3 at room temperature, which is 10 times higher than that of the pure $Ti_3C_2T_x$ sensor. Furthermore, this sensor is endowed with excellent selectivity, reliable long-term stability, and reproducibility. The enhanced sensing performance is associated with the interconnected structure and the synergistic effect of $Ti_3C_2T_x$ and CNH. This work provides an effective way to prepare MXene-based sensitive materials for NH_3 sensors, which shows excellent NH_3 detection potential at room temperature.

KEYWORDS

gas sensors, $Ti_3C_2T_x$, ammonia, MXene, room temperature

1 Introduction

Ammonia (NH_3) detection is important in the industrial environment and for early diagnosis of medical diseases. Excess NH_3 is harmful to human health as it increases the incidence of respiratory and cardiovascular diseases (Li et al., 2016; Achary et al., 2018; Wang et al., 2018; Wu et al., 2019). Long-term exposure may cause blindness or ammonia poisoning in human beings. NH_3 exposure limitations have been set as 35 ppm for 10 min and 25 ppm for 8 h (Fedoruk et al., 2005; Gangopadhyay et al., 2008). In addition, it can be directly life-threatening when the concentrations of NH_3 are up to 300 ppm (Raj et al., 2010). NH_3 is also a natural body metabolite, and high levels of NH_3 in exhaled gas may reflect several liver and lung-related diseases (Narasimhan et al., 2001; Pagonas et al., 2012; Obermeier et al., 2017), which is potentially applied for noninvasive disease diagnostics. The concentration of exhaled NH_3 for healthy people is in the range of 0.4–1.8 ppm, but that in the breath of end-stage renal disease patients is normally beyond 4.9 ppm. Thus, NH_3 sensors can potentially be applied for noninvasive diagnosis of renal disease (Ji et al., 2019).

MXene is a group of transition metal carbides, nitrides, and carbonitrides with a layered structure similar to that of two-dimensional graphene (Su et al., 2022). Due to

their unique surficial and electrical properties, multiple MXenes with a rich chemical composition have a wide range of promising applications in energy storage, hydrogen storage, chemical biosensors, and purification (Zhu et al., 2017; Zhang et al., 2018). $Ti_3C_2T_x$ MXenes with high electrical conductivity, numerous active sites, and abundant terminal functional groups have been widely used as an excellent sensitive material for gas detection at room temperature. The type and number of oxygen-containing functional groups can change the conductivity of $Ti_3C_2T_x$ MXenes and also effectively act as functional sites for gas adsorption. $Ti_3C_2T_x$ MXene is a potential NH_3 -sensitive material (Anasori et al., 2017), which displays more sensitivity to NH_3 than CO_2 , O_2 , and H_2 because the etched $Ti_3C_2T_x$ surface is enriched with oxygen functional groups (Wu et al., 2019). However, pristine $Ti_3C_2T_x$ MXenes with relatively lower capability have rarely been used as sensing materials directly.

The methods to improve the sensor performance mainly include modification of second-phase materials to enhance the activity of the sensitive material or the design of new structures to further promote the practical production applications of gas sensors. The construction of heterostructures effectively improves the gas sensing performance of $Ti_3C_2T_x$ MXene. The electronic properties regulated by the interface of heterostructures may result in enhanced charge transport. Researchers have fabricated the gas sensing materials based on the MXene heterostructures with carbon nanostructures of reduced graphene oxide and carbon nanotubes (Lee et al., 2020; Hassan et al., 2021; Seekaew et al., 2023). These heterostructures combine the high conductivity and structural stability of carbon nanostructures with the merit of $Ti_3C_2T_x$ MXene (Keshtkara et al., 2017). Carbon nanohorn (CNH) is a carbon nanomaterial with an angular appearance and aggregated subspherical shape and has abundant active sites and good electrical conductivity (Zhu et al., 2009; Zhu et al., 2019). It has also been widely used for immunosensing, storage, and electrochemical detection of gases such as methane and hydrogen (Ojeda et al., 2014; Chen et al., 2017; Zheng et al., 2020). Zhou et al. (2022) prepared In_2O_3/CNH nanocomposites and fabricated ideal low-power H_2S gas sensors. Therefore, combining $Ti_3C_2T_x$ MXene with CNH may be promising for improving the sensing properties.

Herein, $Ti_3C_2T_x/CNH$ nanocomposites have been fabricated by an electrostatic self-assembly method. The CNH surface is positively charged by adding the surfactant and then combined with the negatively charged $Ti_3C_2T_x$ via an electrostatic self-assembly method. CNH has a larger specific surface area, providing more reaction sites and gas adsorption capacity, and the gas sensor made of $Ti_3C_2T_x/CNH$ nanocomposite displays good response, excellent selectivity, and reliable stability for NH_3 detection at room temperature.

2 Experimental section

2.1 Preparation of sensing materials

2.1.1 Preparation of $Ti_3C_2T_x$ MXene

For selective etching of Al from Ti_3AlC_2 MAX, we used a mixed etching solution containing hydrochloric acid and sodium fluoride as follows: 2 g Ti_3AlC_2 powder was slowly added to an etching solution composed of 40 mL 6 M hydrochloric acid and 2 g sodium

fluoride (Wu et al., 2019). The mixed dispersion was continuously stirred at 60°C for 48 h in a water bath. The dispersion was then washed with ethanol and deionized water several times to remove the acidic residue until the pH value was 6. The precipitate was dried in a vacuum oven at 60°C for approximately 8 h to obtain the multilayer $Ti_3C_2T_x$ powder. Then, an appropriate amount of $Ti_3C_2T_x$ powder was added to deionized water and dispersed by ultrasonication to obtain 2 mg/mL of $Ti_3C_2T_x$ dispersion.

2.1.2 Synthesis of $Ti_3C_2T_x/CNH$ nanocomposites

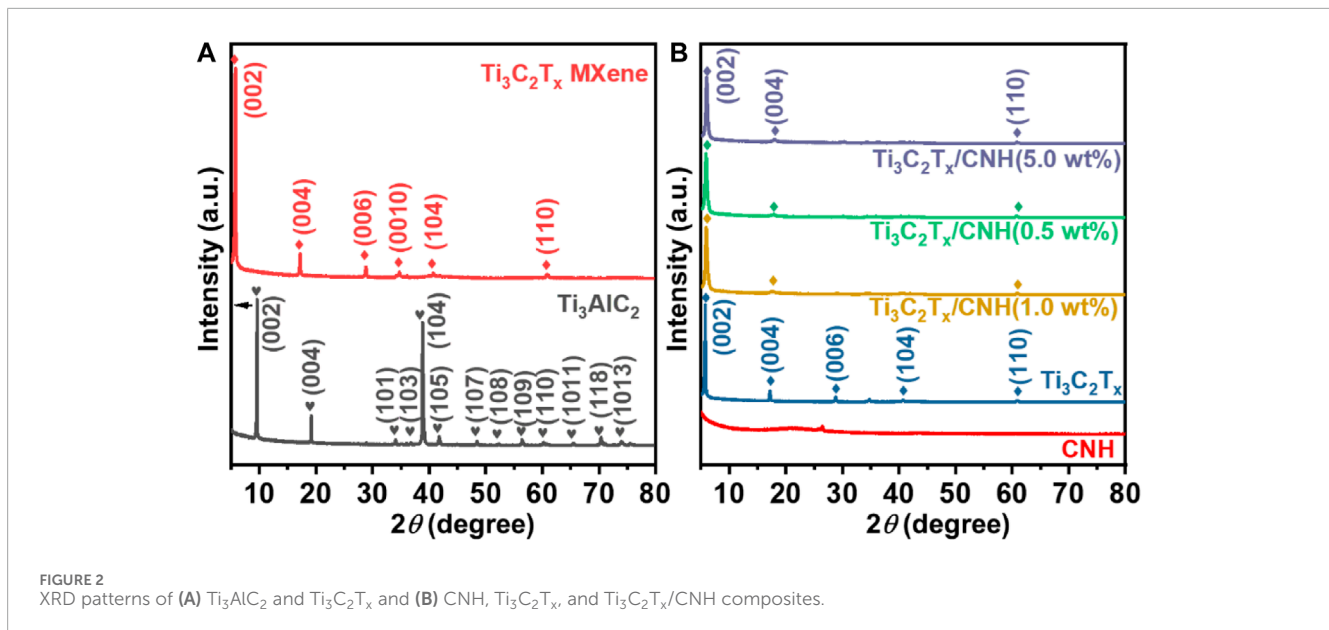
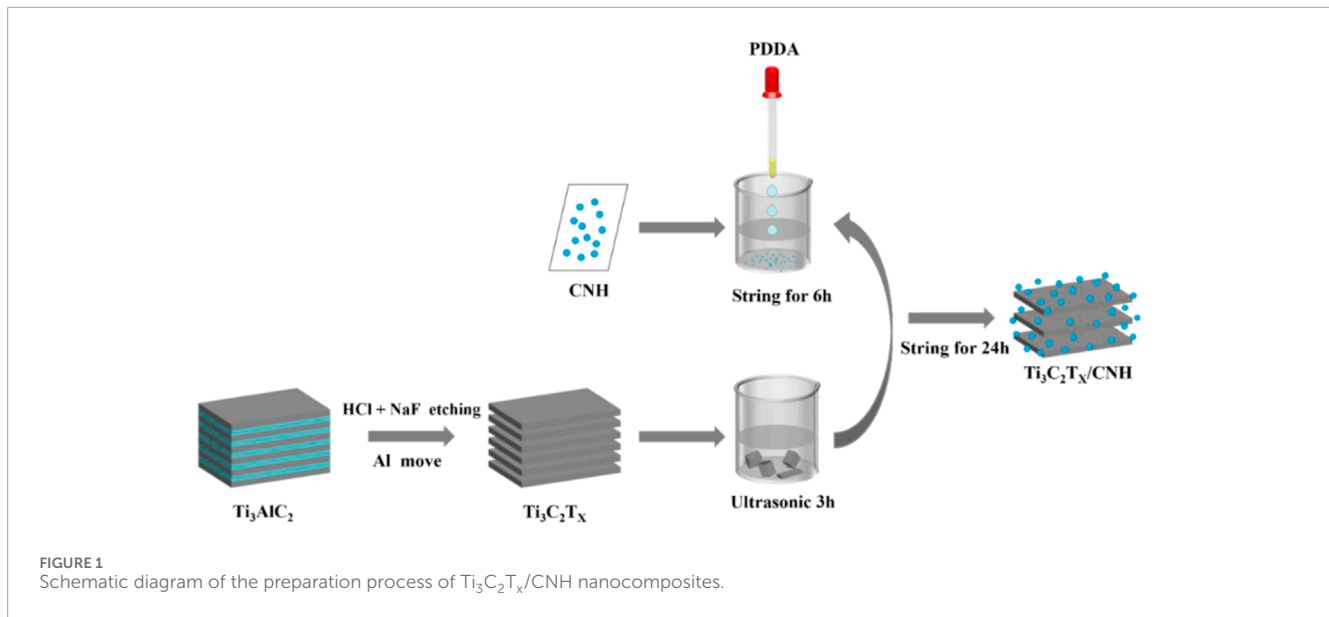
Figure 1 shows the synthesis process of $Ti_3C_2T_x/CNH$ nanocomposites, where $Ti_3C_2T_x/CNH$ nanocomposites were successfully synthesized by an electrostatic self-organization method. CNH was obtained from Henan Yingneng Novel Material Technology Co., Ltd. CNH (50 mg) was dispersed in 10 mL of polydimethylallylammonium chloride (PDDA) and stirred for 6 h at 25°C to obtain positively charged CNH. Then, different amounts of $Ti_3C_2T_x$ were added (CNH accounted for 0.1, 0.5, 1.0, and 5.0 wt%, respectively), and the dispersions were continued to be stirred for 24 h at 25°C. The obtained dispersion was centrifuged and washed with deionized water and ethanol in turn and dried in a vacuum oven to obtain $Ti_3C_2T_x/CNH$ nanocomposites.

2.2 Fabrication and characterization of the gas-sensing devices

The component of the sensor mainly includes a ceramic tube with a gold electrode coated with a sensitive material and a sensor base. The process of fabrication is as follows: the sensitive material is mixed with ethanol and sonicated for 15 min to form a stable dispersion. Then, 5 μ L of the prepared dispersion was uniformly coated on the ceramic tube by using a pipette, and the gold electrode was completely covered to form a sensitive layer. The gas-sensing performance was analyzed at room temperature and 40%–45% relative humidity (RH) by using a CGS-8 analysis system from Elite Technology Co., Ltd. A static gas-blending method was used to obtain the target gases with different concentrations, and the detailed processes have been listed in the previous work (Han et al., 2023). The gas-sensing response is defined as $S = |R_g - R_a|/R_a \times 100\%$, where R_g and R_a represent the sensors' resistance in the target gas and air, respectively (Han et al., 2023; Yao et al., 2023).

2.3 Characterizations

The crystal phases and chemical bonding of the as-prepared materials were analyzed by X-ray powder diffraction (XRD, Rigaku Ultima IV) and X-ray photoelectron spectroscopy (XPS, Shimadzu/Kratos AXIS SUPRA+), respectively. Field-emission scanning electron microscopy (FESEM, JSM-7001F) and transmission electron microscopy (TEM, JEM-F200) were performed to characterize the morphology and microstructure of the sensitive materials, respectively. The Fourier-transform infrared (FT-IR) spectrum was performed on PerkinElmer Spectrum 3.



3 Results and discussion

3.1 Characterizations of sensitive materials

Figure 2A displays the XRD patterns of Ti_3AlC_2 and $\text{Ti}_3\text{C}_2\text{T}_x$ MXene. The typical diffraction peaks of Ti_3AlC_2 -MAX at 9.5, 19.2, 34.1, 36.9, 38.9, 41.8, 48.4, 42.4, 56.5, 60.2, 65.4, 70.2, and 74.0° correspond to (002), (004), (101), (103), (104), (105), (107), (108), (109), (110), (1011), (119), and (1013) crystal planes, respectively (Tian et al., 2022). Compared with Ti_3AlC_2 , the characteristic peaks of the (002) and (004) facets of $\text{Ti}_3\text{C}_2\text{T}_x$ were reduced from $2\theta = 9.5^\circ$ to 5.7° and $2\theta = 19.2^\circ$ to 17.2° , respectively. Furthermore, the appearance of new characteristic peaks at 28.8° for (006) and 34.7° for (0010) also implies successful formation of $\text{Ti}_3\text{C}_2\text{T}_x$. Figure 2B presents the XRD patterns of CNH,

$\text{Ti}_3\text{C}_2\text{T}_x$, and $\text{Ti}_3\text{C}_2\text{T}_x/\text{CNH}$ composites. For the XRD patterns of $\text{Ti}_3\text{C}_2\text{T}_x/\text{CNH}$, the characteristic peaks of $\text{Ti}_3\text{C}_2\text{T}_x$ can be observed in all $\text{Ti}_3\text{C}_2\text{T}_x/\text{CNH}$ composites with different amounts of CNH, but no pronounced CNH peaks can be found for the low CNH content (Zhou et al., 2022).

The morphologies of Ti_3AlC_2 , $\text{Ti}_3\text{C}_2\text{T}_x$, CNH, and $\text{Ti}_3\text{C}_2\text{T}_x/\text{CNH}$ nanocomposites were characterized by FESEM. As shown in Figure 3A, Ti_3AlC_2 has a dense multilayer structure. SEM images of multilayer $\text{Ti}_3\text{C}_2\text{T}_x$ are displayed in Figure 3B, and there is an obvious spacing between the lamellae, a typical accordion-like structure, and a smooth surface. Figure 3C presents the SEM image of CNH nanospheres with an average diameter of 70–110 nm. The morphology of $\text{Ti}_3\text{C}_2\text{T}_x/\text{CNH}$ (0.5 wt%) composite nanomaterials is exhibited in Figure 3D, indicating the successful combination between CNH and $\text{Ti}_3\text{C}_2\text{T}_x$.

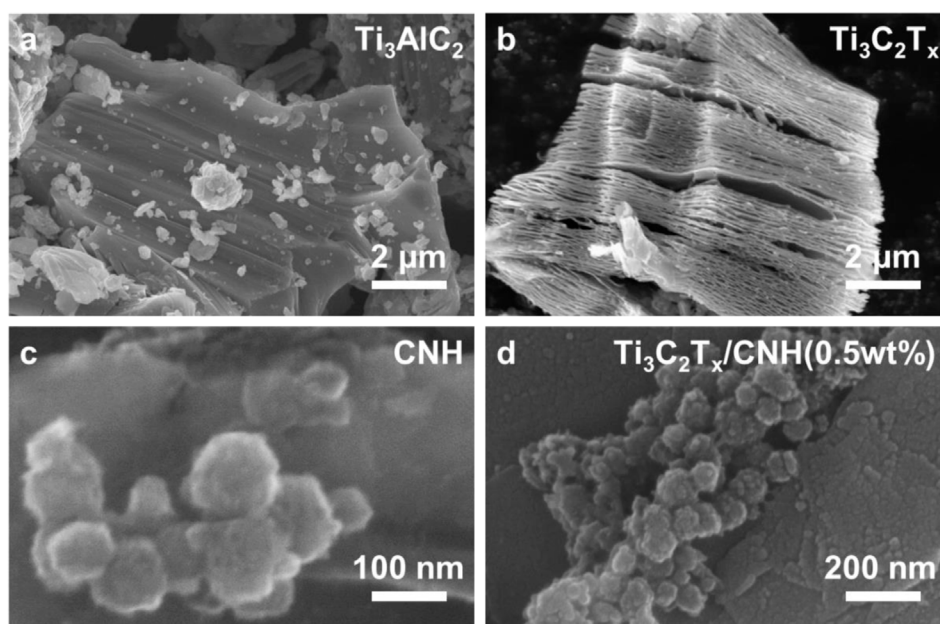


FIGURE 3
FESEM images of the (A) Ti_3AlC_2 , (B) $\text{Ti}_3\text{C}_2\text{T}_x$, (C) CNH, and (D) $\text{Ti}_3\text{C}_2\text{T}_x/\text{CNH}$ (0.5 wt%) nanocomposites.

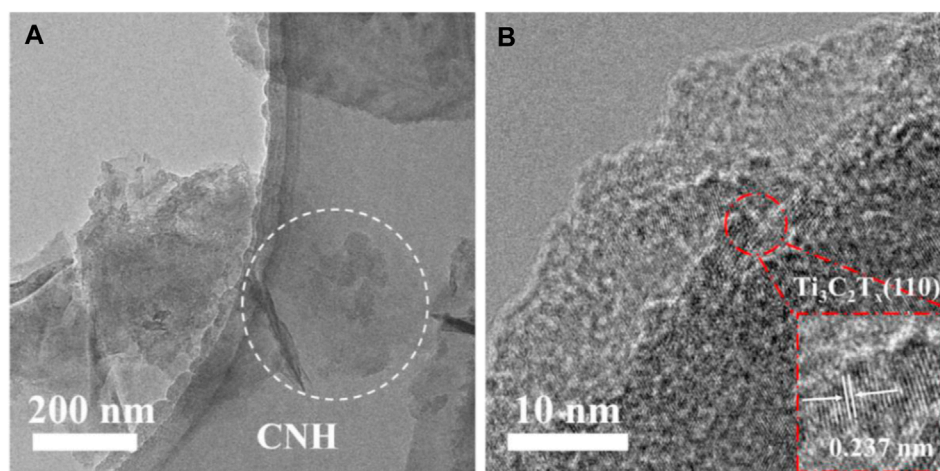


FIGURE 4
(A) TEM image and (B) HRTEM image of the $\text{Ti}_3\text{C}_2\text{T}_x/\text{CNH}$ (0.5 wt%) nanocomposite.

To further investigate the microstructure of the sensitive material, the $\text{Ti}_3\text{C}_2\text{T}_x/\text{CNH}$ sample was characterized by TEM and high-resolution transmission electron microscopy (HRTEM). The TEM images of $\text{Ti}_3\text{C}_2\text{T}_x/\text{CNH}$ (0.5 wt%) in Figure 4A also confirm the successful combination between $\text{Ti}_3\text{C}_2\text{T}_x$ and CNH nanospheres. For $\text{Ti}_3\text{C}_2\text{T}_x/\text{CNH}$, it can be seen that $\text{Ti}_3\text{C}_2\text{T}_x$ is composed of thin sheets with a two-dimensional lamellar structure, and the presence of CNH nanospheres is confirmed. The HRTEM images of the $\text{Ti}_3\text{C}_2\text{T}_x/\text{CNH}$ composites are shown in Figure 4B. The spacing of the lattice surfaces in $\text{Ti}_3\text{C}_2\text{T}_x$ is 0.237 nm, which can be attributed to the (110) crystal plane

of $\text{Ti}_3\text{C}_2\text{T}_x$ (Zhang et al., 2018). The lattice spacing stripes are not obvious due to the poor crystallinity of CNH. The CNH microspheres and $\text{Ti}_3\text{C}_2\text{T}_x$ nanosheets are displayed in Figure 4, which are involved in the successful preparation of $\text{Ti}_3\text{C}_2\text{T}_x/\text{CNH}$ nanocomposites.

The chemical bonding of $\text{Ti}_3\text{C}_2\text{T}_x/\text{CNH}$ samples was further analyzed by XPS, and the corresponding results are exhibited in Figure 5. Figure 5A shows the C 1s spectrum of $\text{Ti}_3\text{C}_2\text{T}_x/\text{CNH}$ with peaks at 293.3, 286.4, 284.8, and 281.4 eV, which are attributed to C=O, C-O, C-C, and C-Ti functional groups, respectively (Zhou et al., 2022). For the O spectrum in Figure 5B, the peak at

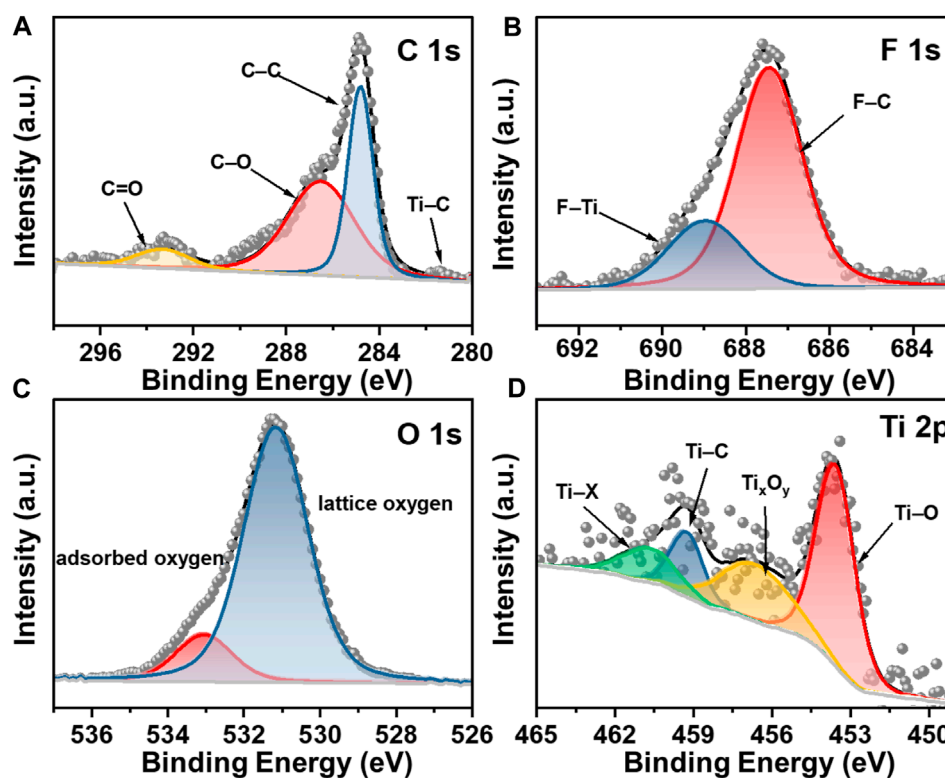


FIGURE 5 (A) C 1s, (B) F 1s, (C) O 1s, and (D) Ti 2p fine spectrum of $\text{Ti}_3\text{C}_2\text{T}_x/\text{CNH}$ (0.5 wt%) composites, respectively.

531.1 eV is typical of surface lattice oxygen, while the peak located at 532.9 eV is characteristic of surface-adsorbed oxygen species (O^{2-} and O^-) (Andreeva et al., 1998; Hu et al., 2018; Lee et al., 2018). The surface-adsorbed oxygen reacts with the target gas molecules through redox reactions, thus effectively enhancing the gas-sensitive properties (Wang et al., 2015). The high-resolution Ti 2p spectrum is displayed in Figure 5C, which corresponds the peaks at 460.7, 459.3, 456.6, and 453.6 eV to Ti-X (Ti^+), T-C (Ti^{2+}), Ti_xO_y (Ti^{3+}), and Ti-O (Ti^{2+}), respectively, where Ti-X corresponds to the sub-stoichiometric ratios of titanium carbide or titanium oxide nitride (Halim et al., 2014). The F 1s spectrum is presented in Figure 5D, and the peaks appearing at 688.9 and 687.5 eV can correspond to F-Ti and F-C, respectively (He et al., 2021). Therefore, the XPS results indicate the successful preparation of $\text{Ti}_3\text{C}_2\text{T}_x/\text{CNH}$ composites, which is consistent with the XRD, SEM, and TEM results. Supplementary Figure S1 shows the FT-IR spectra of $\text{Ti}_3\text{C}_2\text{T}_x$, CNH, and $\text{Ti}_3\text{C}_2\text{T}_x/\text{CNH}$. The bands lower than $1,000\text{ cm}^{-1}$ correspond to the vibrations of Ti-O and C-O. The bands at $1,350$ and $1,630\text{ cm}^{-1}$ may be related to the vibrations of O-H stretching and C=O bonding, respectively (Zhou et al., 2022).

3.2 Gas-sensing performance

To investigate the effect of CNH content on the NH_3 -sensing performance of $\text{Ti}_3\text{C}_2\text{T}_x/\text{CNH}$ sensors, the sensing characteristics of $\text{Ti}_3\text{C}_2\text{T}_x/\text{CNH}$ composite sensors with different CNH contents have been tested at room temperature. Figure 6A shows I - V curves

of the $\text{Ti}_3\text{C}_2\text{T}_x$, CNH, and $\text{Ti}_3\text{C}_2\text{T}_x/\text{CNH}$ (0.5 wt%) sensors, which display the typical Ohmic contacts, and thus, the resistances of the gas sensors are decided by the sensitive materials rather than the contact characteristics (Yuan et al., 2018; Han et al., 2021). As shown in Figure 6B, Supplementary Figure S2, the responses of pure $\text{Ti}_3\text{C}_2\text{T}_x$, CNH, $\text{Ti}_3\text{C}_2\text{T}_x/\text{CNH}$ (0.1 wt%), $\text{Ti}_3\text{C}_2\text{T}_x/\text{CNH}$ (0.5 wt%), $\text{Ti}_3\text{C}_2\text{T}_x/\text{CNH}$ (1.0 wt%), and $\text{Ti}_3\text{C}_2\text{T}_x/\text{CNH}$ (5.0 wt%) sensors to 100 ppm NH_3 are 2.0, 8.7, 21.6, 10.8, and 8.7%, respectively. The $\text{Ti}_3\text{C}_2\text{T}_x/\text{CNH}$ (0.5 wt%) sensor is endowed with the highest response, which is approximately 10 times the response value of previously reported $\text{Ti}_3\text{C}_2\text{T}_x$ -based sensors, indicating that CNH nanospheres significantly enhance the response to NH_3 (Wu et al., 2019). As the CNH content increases, the response to NH_3 increases accordingly, and the best peak-response ($\sim 21.6\%$) is obtained at a CNH content of 0.5 wt%, indicating that the cooperation between $\text{Ti}_3\text{C}_2\text{T}_x$ and CNH significantly enhances the NH_3 -response. However, as the CNH content in the composite continues to increase, the response of the composite to NH_3 decreases instead. It may be because CNH has a large specific surface area, which can provide more reactive sites and help in improving the gas-sensitive response, while excess CNH covered with $\text{Ti}_3\text{C}_2\text{T}_x$ decreases the number of reactive sites on the $\text{Ti}_3\text{C}_2\text{T}_x$ surface, which affects the adsorption of NH_3 by $\text{Ti}_3\text{C}_2\text{T}_x$. Selectivity is considered to be an important key metric for evaluating gas sensors. The response and recovery time of the gas sensor are important parameters to be examined when the sensor is used in practice. As shown in Figure 6C, when the gas sensor is

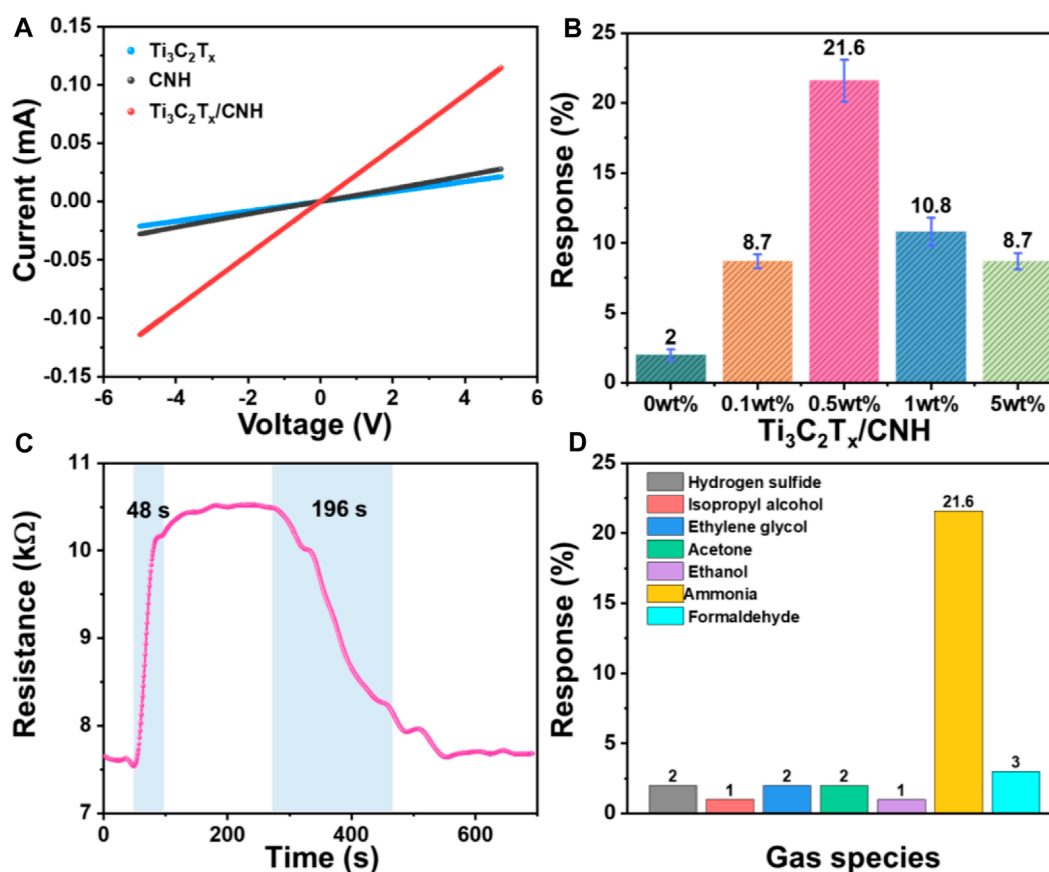


FIGURE 6

(A) I–V curves of comparison of $\text{Ti}_3\text{C}_2\text{T}_x$, CNH, and $\text{Ti}_3\text{C}_2\text{T}_x/\text{CNH}$ (0.5 wt%). (B) Response of different ratios of $\text{Ti}_3\text{C}_2\text{T}_x/\text{CNH}$ samples to 100 ppm NH_3 at room temperature. (C) Dynamic response/recovery characteristic of the $\text{Ti}_3\text{C}_2\text{T}_x/\text{CNH}$ (0.5 wt%) sensor to 100 ppm NH_3 at room temperature. (D) Response of the $\text{Ti}_3\text{C}_2\text{T}_x/\text{CNH}$ (0.5 wt%) sensor to different gases at 100 ppm.

TABLE 1 Comparison of the $\text{Ti}_3\text{C}_2\text{T}_x/\text{CNH}$ sensor with the reported $\text{Ti}_3\text{C}_2\text{T}_x$ -based NH_3 sensors.

Materials	Concentration (ppm)	Response (%)	Ref
$\text{Ti}_3\text{C}_2\text{T}_x$	100	$\Delta R/R_0 = 0.8$	Kim et al. (2018)
$\text{Ti}_3\text{C}_2\text{T}_x/\text{PU}$ fibers	10	$\Delta R/R_0 = 0.6$	Tang et al. (2021)
$\text{Ti}_3\text{C}_2\text{T}_x/\text{graphene}$ fibers	50	$\Delta R/R_0 = 6.8$	Lee et al. (2020)
Alkalized $\text{Ti}_3\text{C}_2\text{T}_x$	100	$\Delta R/R_0 = 28.9$	Yang et al. (2019)
$\text{Ti}_3\text{C}_2\text{T}_x$	100	$\Delta R/R_0 = 21$	Lee et al. (2017)
Na- $\text{Ti}_3\text{C}_2\text{T}_x$	100	$\Delta R/R_0 = 0.4$	Kim et al. (2021)
3D $\text{Ti}_3\text{C}_2\text{T}_x$	10	$\Delta R/R_0 = 0.7$	Yuan et al. (2018)
$\text{Ti}_3\text{C}_2\text{T}_x/\text{CNH}$	100	$\Delta R/R_0 = 21.6$	This work

exposed to 100 ppm NH_3 , the resistance value of the gas-sensing element reaches 90% of the equilibrium value in about 48 s, and the sensor recovery time is calculated as 196 s (Chen et al., 2022). The response of the $\text{Ti}_3\text{C}_2\text{T}_x/\text{CNH}$ (0.5 wt%) sensor at room temperature to various interfering gases at 100 ppm is

displayed in Figure 6D. The sensor has responses of 2, 1, 2, 1, 21.6, and 3% to 100 ppm hydrogen sulfide, isopropyl alcohol, ethylene glycol, acetone, ethanol, ammonia, and formaldehyde, respectively. The $\text{Ti}_3\text{C}_2\text{T}_x/\text{CNH}$ -based sensor shows excellent selectivity for NH_3 gas. As listed in Table 1, the response of the

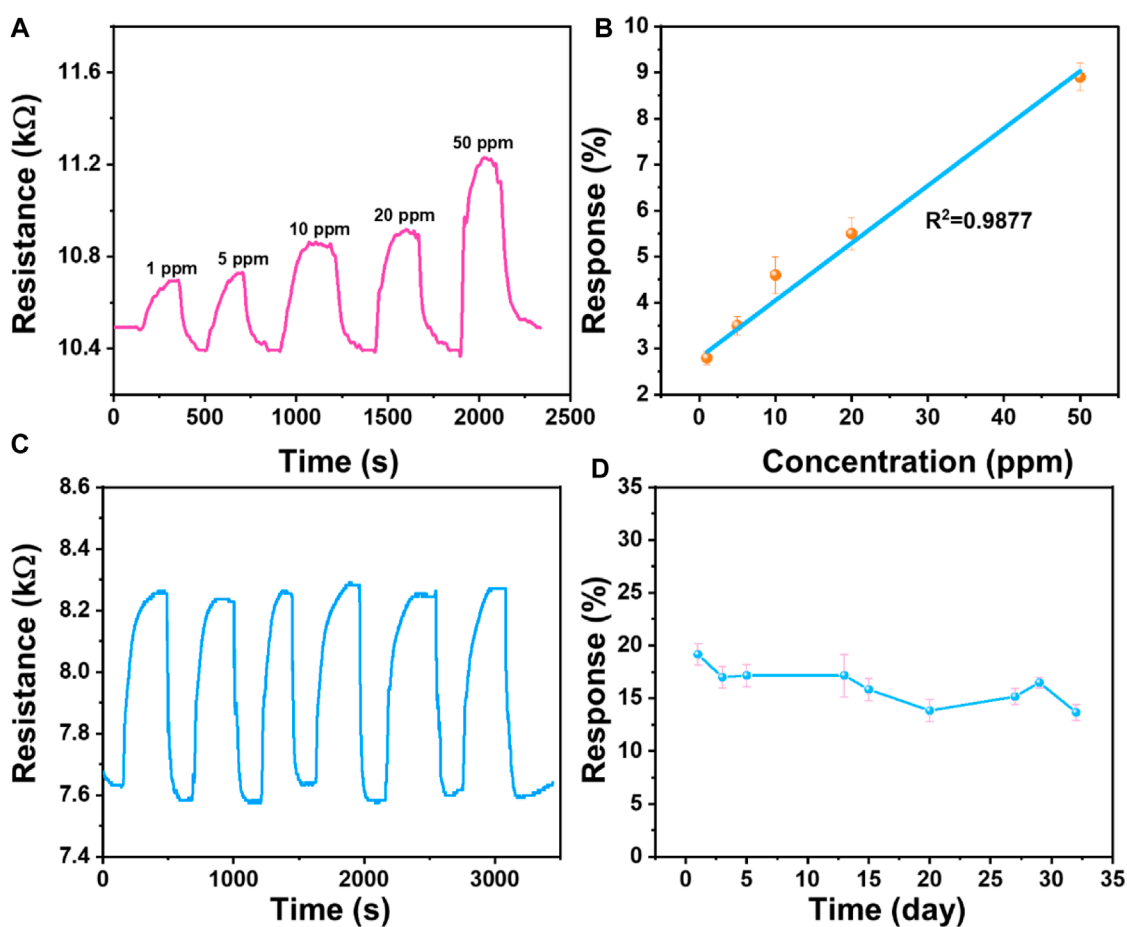


FIGURE 7 (A) Dynamic response/recovery curve of the $\text{Ti}_3\text{C}_2\text{T}_x/\text{CNH}$ (0.5 wt%) sensor at room temperature for a concentration range of 1–50 ppm NH_3 . (B) Fitting curves between gas concentrations and response values of the $\text{Ti}_3\text{C}_2\text{T}_x/\text{CNH}$ (0.5 wt%) sensor. (C) Repeatability of the $\text{Ti}_3\text{C}_2\text{T}_x/\text{CNH}$ (0.5 wt%) sensor to 50 ppm NH_3 for six continuous cycles. (D) Long-term stability of the $\text{Ti}_3\text{C}_2\text{T}_x/\text{CNH}$ (0.5 wt%) sensor to 100 ppm NH_3 .

$\text{Ti}_3\text{C}_2\text{T}_x/\text{CNH}$ -based sensor is competitive with that of the reported $\text{Ti}_3\text{C}_2\text{T}_x$ -based NH_3 sensors.

The dynamic response of the optimal $\text{Ti}_3\text{C}_2\text{T}_x/\text{CNH}$ (0.5 wt%) sensor to different concentrations (1–50 ppm) of NH_3 gas is displayed in Figure 7A. Figure 7B shows that the corrected curve is almost linear, with a correlation coefficient R^2 of 0.9877. The detection limit of this $\text{Ti}_3\text{C}_2\text{T}_x/\text{CNH}$ sensor is calculated to be about 250 ppb (Han et al., 2023). The response of the $\text{Ti}_3\text{C}_2\text{T}_x/\text{CNH}$ (0.5 wt%) gas sensor increases linearly with increasing NH_3 concentration, showing a good linearity. Reproducibility and long-term stability are also important indexes in the practical application of the sensor. Exposure of the sensor to 50 ppm NH_3 has been performed for six consecutive cycles at room temperature (Figure 7C). The results show that the composite sensor has good cycling reproducibility with no significant change in NH_3 detection during the continuous adsorption–desorption process. Moreover, as shown in Figure 7D, the stable response of the sensor to 100 ppm NH_3 over 30 days indicates that the device also exhibits relatively good long-term stability. Furthermore, Supplementary Figure S3 shows the response/recovery characteristics of the $\text{Ti}_3\text{C}_2\text{T}_x/\text{CNH}$ sensor to 50 ppm NH_3 at 20, 40, and 55% RH conditions. The results

show that the response values of the $\text{Ti}_3\text{C}_2\text{T}_x/\text{CNH}$ sensor to 50 ppm NH_3 remain stable at about 10% within the RH range of 20%–55%.

3.3 Gas-sensing mechanisms

The improved gas-sensing performance of the $\text{Ti}_3\text{C}_2\text{T}_x/\text{CNH}$ (0.5 wt%)-based sensor for NH_3 can be explained by the following aspects:

$\text{Ti}_3\text{C}_2\text{T}_x$ has abundant and active surface termination groups, which is beneficial for the sensing performance. The decorated CNH can provide more adsorption sites for the target gas, and the loading of CNH particles on the surface and interlayers of $\text{Ti}_3\text{C}_2\text{T}_x$ nanosheets slows down the accumulation of layered $\text{Ti}_3\text{C}_2\text{T}_x$ nanosheets and increases the $\text{Ti}_3\text{C}_2\text{T}_x$ nanosheet layer spacing. Compared with pure $\text{Ti}_3\text{C}_2\text{T}_x$, the loaded CNH increases the specific surface area of $\text{Ti}_3\text{C}_2\text{T}_x/\text{CNH}$ composites, improves the adsorption and diffusion of NH_3 , and contributes to the improved NH_3 -response.

A schematic diagram of the gas-sensing mechanism of the $\text{Ti}_3\text{C}_2\text{T}_x/\text{CNH}$ sensor is displayed in Figures 8A, B. $\text{Ti}_3\text{C}_2\text{T}_x$ exhibits

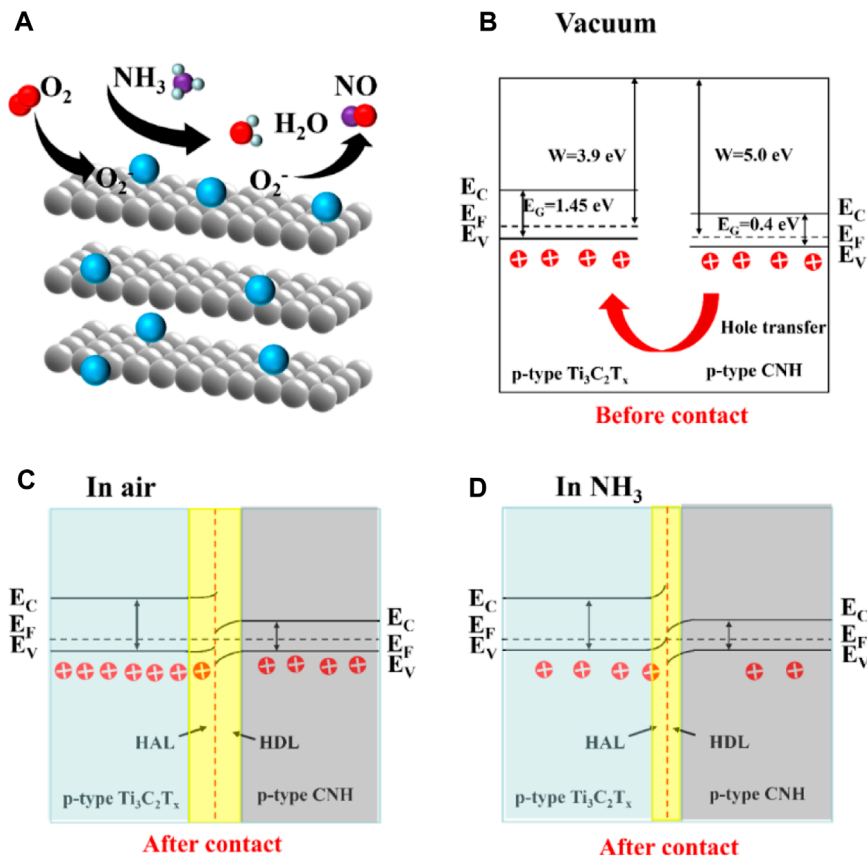
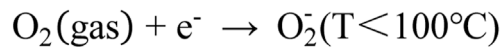
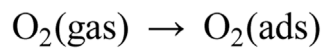


FIGURE 8

Schematic diagram of (A) the gas-sensing mechanism of the $\text{Ti}_3\text{C}_2\text{T}_x/\text{CNH}$ sensor, (B) energy band diagram of $\text{Ti}_3\text{C}_2\text{T}_x$ and CNH before forming a complex, and energy band structure of $\text{Ti}_3\text{C}_2\text{T}_x/\text{CNH}$ composite in (C) air and (D) NH_3 .

p-type sensing behavior, and the relevant literature shows that its bandgap is 1.45 eV. CNH is a p-type semiconductor with a bandgap of 0.4 eV. The work functions of $\text{Ti}_3\text{C}_2\text{T}_x$ and CNH are 3.9 and 5.0 eV, respectively (Lee et al., 2017; Schultz et al., 2019; Zhou et al., 2022). As shown in Figure 8C, in the $\text{Ti}_3\text{C}_2\text{T}_x/\text{CNH}$ nanocomposite, nanoscale p-p heterojunctions are formed between $\text{Ti}_3\text{C}_2\text{T}_x$ and CNH. Since the work function of CNH is higher than that of $\text{Ti}_3\text{C}_2\text{T}_x$, electrons will flow from the latter to the former, resulting in the formation of a hole depletion layer (HDL) in CNH and a hole accumulation layer (HAL) in $\text{Ti}_3\text{C}_2\text{T}_x$ (Yao et al., 2023).

In air, oxygen molecules are adsorbed on the surface of the composite (Eqs 1 and 2). The oxygen molecules adsorb on the CNH surface, and the negative charge formed on the surface will increase its work function, thus increasing the work function difference between CNH and $\text{Ti}_3\text{C}_2\text{T}_x$. This will require transfer of more electrons to compensate. As a result, the HAL thickness in $\text{Ti}_3\text{C}_2\text{T}_x$ increases, and the resistance of the sensor in air is relatively low. When the composite is exposed to NH_3 , the NH_3 molecules react with O_2^- species, releasing electrons to neutralize the holes (Figure 8D, Eq. 3), reducing the hole density in the nanocomposite, and disrupting the dynamic carrier balance between $\text{Ti}_3\text{C}_2\text{T}_x$ and CNH.

The hole transfer from CNH to $\text{Ti}_3\text{C}_2\text{T}_x$ reduces the thickness of HAL on the CNH surface. The thinner HAL at the heterojunction interface contributes to increased sensor resistance (Suh et al., 2018).



4 Conclusion

$\text{Ti}_3\text{C}_2\text{T}_x/\text{CNH}$ nanocomposites have been prepared by an electrostatic self-assembly method, and the characterization and gas-sensitive sensing properties of the material are investigated. The experimental results show the $\text{Ti}_3\text{C}_2\text{T}_x/\text{CNH}$ (0.5 wt%) nanocomposite sensor has good gas-sensing performance for NH_3 gas at room temperature, indicating that CNH can effectively optimize the sensor and make $\text{Ti}_3\text{C}_2\text{T}_x$ MXene more suitable for detecting NH_3 at room temperature.

Data availability statement

The original contributions presented in the study are included in the article/Supplementary Material; further inquiries can be directed to the corresponding author.

Author contributions

YH: writing–review and editing, conceptualization, funding acquisition, investigation, and writing–original draft. YD:

writing–original draft. YY: writing–review and editing. ZL: writing–review and editing. ZZ: writing–review and editing.

Funding

The author(s) declare that financial support was received for the research, authorship, and/or publication of this article. The authors gratefully acknowledge financial supports by the National Natural Science Foundation of China (62104149) and the Shanghai Sailing Program (21YF1431400).

Conflict of interest

The authors declare that the research was conducted in the absence of any commercial or financial relationships that could be construed as a potential conflict of interest.

Publisher's note

All claims expressed in this article are solely those of the authors and do not necessarily represent those of their affiliated organizations, or those of the publisher, the editors, and the reviewers. Any product that may be evaluated in this article, or claim that may be made by its manufacturer, is not guaranteed or endorsed by the publisher.

Supplementary material

The Supplementary Material for this article can be found online at: <https://www.frontiersin.org/articles/10.3389/fmats.2024.1383538/full#supplementary-material>

References

- Achary, L. S. K., Kumar, A., Barik, B., Nayak, P. S., Tripathy, N., Kar, J. P., et al. (2018). Reduced graphene oxide-CuFe₂O₄ nanocomposite: a highly sensitive room temperature NH₃ gas sensor. *Sens. Actuators B* 272, 100–109. doi:10.1016/j.snb.2018.05.093
- Anasori, B., Lukatskaya, M. R., and Gogotsi, Y. (2017). 2D metal carbides and nitrides (MXenes) for energy storage. *Nat. Rev. Mat.* 2 (2), 16098. doi:10.1038/natrevmats.2016.98
- Andreeva, D., Tabakova, T., Idakiev, V., Christov, P., and Giovanoli, R. (1998). Au/ α -Fe₂O₃ catalyst for water–gas shift reaction prepared by deposition–precipitation. *Appl. Catal. A* 169 (1), 9–14. doi:10.1016/s0926-860x(97)00302-5
- Chen, C., Jiang, M., Luo, X., Tai, H., Jiang, Y., Yang, M., et al. (2022). Ni-Co-P hollow nanobricks enabled humidity sensor for respiratory analysis and human-machine interfacing. *Sens. Actuators, B* 370, 132441. doi:10.1016/j.snb.2022.132441
- Chen, J., He, P., Bai, H., Lei, H., Liu, K., Dong, F., et al. (2017). Novel phosphomolybdenic acid/single-walled carbon nanohorn-based modified electrode for non-enzyme glucose sensing. *J. Electroanal. Chem.* 784, 41–46. doi:10.1016/j.jelechem.2016.12.003
- Fedoruk, M. J., Bronstein, R., and Kerger, B. D. (2005). Ammonia exposure and hazard assessment for selected household cleaning product uses. *J. Expo. Anal. Environ. Epidemiol.* 15 (6), 534–544. doi:10.1038/sj.jea.7500431
- Gangopadhyay, R. K., and Das, S. K. (2008). Ammonia leakage from refrigeration plant and the management practice. *Process Saf. Prog.* 27 (1), 15–20. doi:10.1002/prs.10208
- Halim, J., Lukatskaya, M. R., Lu, J., Cook, K. M., Smith, C. R., Näslund, L. Å., et al. (2014). Transparent conductive two-dimensional titanium carbide epitaxial thin films. *Chem. Mat.* 26 (7), 2374–2381. doi:10.1021/cm500641a
- Han, Y., Ding, Y., Zhang, W., Zhuang, H., Wang, Z., Li, Z., et al. (2023). SnS₂/Ti₃C₂T_x hybrids for conductometric triethylamine detection at room temperature. *Sens. Actuators, B* 381, 133360. doi:10.1016/j.snb.2023.133360
- Han, Y., Liu, Y., Su, C., Chen, X., Li, B., Jiang, W., et al. (2021). Hierarchical WS₂-WO₃ nanohybrids with P–N heterojunctions for NO₂ detection. *ACS Appl. Nano Mat.* 4, 1626–1634. doi:10.1021/acsnm.0c03094
- Hassan, K., Stanley, N., Tung, T., Yap, P. L., Rastin, H., Yu, L., et al. (2021). Extrusion-printed CNT-graphene sensor array with embedded MXene/PEDOT:PSS heater for enhanced NO₂ sensing at low temperature. *Adv. Mat. Interfaces* 8, 2101175. doi:10.1002/admi.202101175
- He, T., Liu, W., Lv, T., Ma, M., Liu, Z., Vasiliev, A., et al. (2021). MXene/SnO₂ heterojunction based chemical gas sensors. *Sens. Actuators, B* 329, 129275. doi:10.1016/j.snb.2020.129275
- Hu, X., Zhu, Z., Li, Z., Xie, L., Wu, Y., and Zheng, L. (2018). Heterostructure of CuO microspheres modified with CuFe₂O₄ nanoparticles for highly sensitive H₂S gas sensor. *Sens. Actuators, B* 264, 139–149. doi:10.1016/j.snb.2018.02.110
- Ji, H., Zeng, W., and Li, Y. (2019). Gas sensing mechanisms of metal oxide semiconductors: a focus review. *Nanoscale* 11 (47), 22664–22684. doi:10.1039/c9nr07699a
- Keshtkara, S., Rashidib, A., and Kootia, M. (2017). Development of tin dioxide quantum dots/multi-walled carbon nanotubes and tin dioxide quantum dots/carbon

- nanohorns nanohybrids as low temperatures natural gas sensors. *Ceram. Int.* 41, 4314326–4314333. doi:10.1016/j.ceramint.2017.07.188
- Kim, S., Lee, J., Doo, S., Kang, Y. C., and Koo, C. M. (2021). Metal-ion-intercalated MXene nanosheet films for NH₃ gas detection. *ACS Appl. Nano Mat.* 4, 14249–14257. doi:10.1021/acsnm.1c03814
- Kim, S. J., Koh, H.-J., Ren, C. E., Kwon, O., Maleski, K., Cho, S. Y., et al. (2018). Metallic Ti₃C₂T_x MXene gas sensors with ultrahigh signal-to-noise ratio. *ACS Nano* 12, 986–993. doi:10.1021/acsnano.7b07460
- Lee, E., VahidMohammadi, A., Prorok, B. C., Yoon, Y. S., Beidaghi, M., and Kim, D. J. (2017). Room temperature gas sensing of two-dimensional titanium carbide (MXene). *ACS Appl. Mat. Interfaces* 9 (42), 37184–37190. doi:10.1021/acsnm.7b11055
- Lee, J., Kim, S. Y., Yoo, H. S., and Lee, W. (2022). Pd-WO₃ chemiresistive sensor with reinforced self-assembly for hydrogen detection at room temperature. *Sens. Actuators, B* 368, 132236. doi:10.1016/j.snb.2022.132236
- Lee, S., Eom, W., Shin, H., Ambade, R. B., Bang, J. H., Kim, H. W., et al. (2020). Room-temperature, highly durable Ti₃C₂T_x MXene/graphene hybrid fibers for NH₃ gas sensing. *ACS Appl. Mat. Interfaces* 12, 10434–10442. doi:10.1021/acsnm.9b21765
- Li, Y., Ban, H., and Yang, M. (2016). Highly sensitive NH₃ gas sensors based on novel polypyrrole-coated SnO₂ nanosheet nanocomposites. *Sens. Actuators B* 224, 449–457. doi:10.1016/j.snb.2015.10.078
- Narasimhan, L. R., Goodman, W., and Patel, C. K. N. (2001). Correlation of breath ammonia with blood urea nitrogen and creatinine during hemodialysis. *Proc. Natl. Acad. Sci.* 98 (8), 4617–4621. doi:10.1073/pnas.071057598
- Obermeier, J., Trefz, P., Happ, J., Schubert, J. K., Staude, H., Fischer, D. C., et al. (2017). Exhaled volatile substances mirror clinical conditions in pediatric chronic kidney disease. *PLoS One* 12 (6), e0178745. doi:10.1371/journal.pone.0178745
- Ojeda, I., Garcinuño, B., Moreno-Guzmán, M., González-Cortés, A., Yudasaka, M., Iijima, S., et al. (2014). Carbon nanohorns as a scaffold for the construction of disposable electrochemical immunosensing platforms application to the determination of fibrinogen in human plasma and urine. *Anal. Chem.* 86 (15), 7749–7756. doi:10.1021/ac501681n
- Pagonas, N., Vautz, W., Seifert, L., Slodzinski, R., Jankowski, J., Zidek, W., et al. (2012). Volatile organic compounds in uremia. *PLoS One* 7 (9), e46258. doi:10.1371/journal.pone.0046258
- Raj, V. B., Nimal, A. T., Parmar, Y., Sharma, M., Sreenivas, K., and Gupta, V. (2010). Cross-sensitivity and selectivity studies on ZnO surface acoustic wave ammonia sensor. *Sens. Actuators, B* 147 (2), 517–524. doi:10.1016/j.snb.2010.03.079
- Schultz, T., Frey, N. C., Hantanasirisakul, K., Park, S., May, S. J., Shenoy, V. B., et al. (2019). Surface termination dependent work function and electronic properties of Ti₃C₂T_x MXene. *Chem. Mat.* 31 (17), 6590–6597. doi:10.1021/acs.chemmater.9b00414
- Seekaew, Y., Kamlue, S., and Wongchoosuk, C. (2023). Room-temperature ammonia gas sensor based on Ti₃C₂T_x MXene/graphene oxide/CuO/ZnO nanocomposite. *ACS Appl. Nano Mat.* 6, 9008–9020. doi:10.1021/acsnm.3c01637
- Su, Y., Li, W., Cheng, X., Zhou, Y., Yang, S., Zhang, X., et al. (2022). High-performance piezoelectric composites via β phase programming. *Nat. Commun.* 13 (4867), 1–12. doi:10.1038/s41467-022-32518-3
- Suh, J. M., Sohn, W., Shim, Y.-S., Choi, J. S., Song, Y. G., Kim, T. L., et al. (2018). P-p heterojunction of nickel oxide-decorated cobalt oxide nanorods for enhanced sensitivity and selectivity toward volatile organic compounds. *ACS Appl. Mat. Interfaces* 10 (1), 1050–1058. doi:10.1021/acsnm.7b14545
- Tian, X., Yao, L., Cui, X., Zhao, R., Chen, T., Xiao, X., et al. (2022). A two-dimensional Ti₃C₂T_x MXene@TiO₂/MoS₂ heterostructure with excellent selectivity for the room temperature detection of ammonia. *J. Mat. Chem. A* 10 (10), 5505–5519. doi:10.1039/d1ta10773a
- Wang, J., Li, Z., Zhang, S., Yan, S., Cao, B., Wang, Z., et al. (2018). Enhanced NH₃ gas-sensing performance of silica modified CeO₂ nanostructure based sensors. *Sens. Actuators, B* 255, 862–870. doi:10.1016/j.snb.2017.08.149
- Wang, S., Zhang, J., Yang, J., Gao, X., Zhang, H., Wang, Y., et al. (2015). Spinel ZnFe₂O₄ nanoparticle-decorated rod-like ZnO nanoheterostructures for enhanced gas sensing performances. *RSC Adv.* 5 (13), 10048–10057. doi:10.1039/c4ra14033h
- Wu, M., He, M., Hu, Q., Wu, Q., Sun, G., Xie, L., et al. (2019). Ti₃C₂ MXene-based sensors with high selectivity for NH₃ detection at room temperature. *ACS Sens.* 4 (10), 2763–2770. doi:10.1021/acssensors.9b01308
- Yang, Z., Liu, A., Wang, C., Liu, F., He, J., Li, S., et al. (2019). Improvement of gas and humidity sensing properties of organ-like MXene by alkaline treatment. *ACS Sens.* 4, 1261–1269. doi:10.1021/acssensors.9b00127
- Yao, Y., Li, Z., Han, Y., Xie, L., Zhao, X., and Zhu, Z. (2023). Fabrication and characterization of a MnO₂/Ti₃C₂T_x based gas sensor for highly sensitive and selective detection of lung cancer marker hexanal. *Chem. Eng. J.* 451, 139029. doi:10.1016/j.cej.2022.139029
- Yuan, W., Yang, K., Peng, H., Li, F., and Yin, F. (2018). A flexible VOCs sensor based on a 3D MXene framework with a high sensing performance. *J. Mat. Chem. A* 6, 18116–18124. doi:10.1039/c8ta06928j
- Zhang, Y., Guo, B., Hu, L., Xu, Q., Li, Y., Liu, D., et al. (2018). Synthesis of SnS nanoparticle-modified MXene (Ti₃C₂T_x) composites for enhanced sodium storage. *J. Alloys Compd.* 732, 448–453. doi:10.1016/j.jallcom.2017.10.223
- Zhang, Y., Wang, L., Zhang, N., and Zhou, Z. (2018). Adsorptive environmental applications of MXene nanomaterials: a review. *RSC Adv.* 8 (36), 19895–19905. doi:10.1039/c8ra03077d
- Zheng, W., Liu, Y., Yang, P., Chen, Y., Tao, J., Hu, J., et al. (2020). Carbon nanohorns enhanced electrochemical properties of Cu-based metal organic framework for ultrasensitive serum glucose sensing. *J. Electroanal. Chem.* 862, 114018. doi:10.1016/j.jelechem.2020.114018
- Zhou, M., Yao, Y., Han, Y., Xie, L., Zhao, X., Barsan, N., et al. (2022). Ultrasensitive gas sensor based on nanocube In₂O₃-CNH composite at low operating temperature. *Sens. Actuators, B* 354, 131224. doi:10.1016/j.snb.2021.131224
- Zhu, G., Fiston, M. N., Qian, J., and Kingsford, O. J. (2019). Highly sensitive electrochemical sensing of para-chloronitrobenzene using a carbon nanohorn-nanotube hybrid modified electrode. *Anal. Methods* 11 (8), 1125–1130. doi:10.1039/c8ay02680g
- Zhu, J., Ha, E., Zhao, G., Zhou, Y., Huang, D., Yue, G., et al. (2017). Recent advance in MXenes: a promising 2D material for catalysis, sensor and chemical adsorption. *Coord. Chem. Rev.* 352, 306–327. doi:10.1016/j.ccr.2017.09.012
- Zhu, S., Li, H., Niu, W., and Xu, G. (2009). Simultaneous electrochemical determination of uric acid, dopamine, and ascorbic acid at single-walled carbon nanohorn modified glassy carbon electrode. *Biosens. Bioelectron.* 25 (4), 940–943. doi:10.1016/j.bios.2009.08.022